Revealing the frictional transition in shear-thickening suspensions

Cécile Clavaud[a,1], Antoine Bérut[a], Bloen Metzger[a], and Yoël Forterre[a]

[a]Aix Marseille Univ, CNRS, Institut Universitaire des Systèmes Thermiques et Industriels, 13453 Marseille, France

Edited by Corey S. O'Hern, Yale University, New Haven, CT, and accepted by Editorial Board Member Pablo G. Debenedetti April 6, 2017 (received for review March 8, 2017)

Shear thickening in dense particulate suspensions was recently proposed to be driven by the activation of friction above an onset stress needed to overcome repulsive forces between particles. Testing this scenario represents a major challenge because classical rheological approaches do not provide access to the frictional properties of suspensions. Here we adopt a different strategy inspired by pressure-imposed configurations in granular flows that specifically gives access to this information. By investigating the quasi-static avalanche angle, compaction, and dilatancy effects in different nonbuoyant suspensions flowing under gravity, we demonstrate that particles in shear-thickening suspensions are frictionless under low confining pressure. Moreover, we show that tuning the range of the repulsive force below the particle roughness suppresses the frictionless state and also the shear-thickening behavior of the suspension. These results, which link microscopic contact physics to the suspension macroscopic rheology, provide direct evidence that the recent frictional transition scenario applies in real suspensions.

soft matter | shear thickening | dense suspensions | friction

Discontinuous shear thickening occurs in suspensions whose viscosity dramatically increases, sometimes by several orders of magnitude, when the imposed shear rate exceeds a critical value (1). The archetype of such suspensions is cornstarch immersed in water. When sheared vigorously or under impact, these fluids suddenly turn into solids (2). Such remarkable properties play a key role in the flowing behavior of modern concrete (3) and have motivated applications ranging from soft-body protections to sports equipment (4). They also offer promising perspectives for the design of smart fluids with tunable rheology (5). However, the potential realm of development and applications remains largely underexplored due to the lack of understanding of this transition (6).

This situation has improved very recently due to new theoretical and numerical works (7, 8). Because non-Brownian suspensions of hard frictional particles immersed in a viscous fluid are Newtonian, as imposed by dimensional analysis (8–10), the key idea of these studies is to add a short-range repulsive force between particles in addition to hydrodynamics and contact forces. This repulsive force can, for instance, stem from electrostatic charges or from a specific coating of polymers on the surface of the particle (11). At small shear rate (or small stress), the repulsive force prevents the grains from coming into contact; the suspension thus flows easily as if particles were frictionless. In the remainder of this paper, this state is referred to as frictionless. The viscosity of such a frictionless suspension would diverge at random close packing, whose volume fraction is $\phi_{\mathrm{rcp}} = 0.64$ for monodisperse spheres. Conversely, at large shear rate (or large stress), the repulsive force is overcome by the hydrodynamic forces and particles are therefore pressed into frictional contacts. The viscosity of such a suspension of frictional particles instead diverges at a lower critical volume fraction $\phi_c < \phi_{\mathrm{rcp}}$, with typically $\phi_c \simeq 0.58$ for monodisperse frictional spheres (9, 10, 12). In essence, the frictional transition described above brings the suspension closer to its jamming point: This critical volume fraction shift suddenly increases its apparent viscosity.

This scenario has been successfully tested and analyzed in discrete numerical simulations performed for non-Brownian (7, 10) and Brownian (13) suspensions. Supporting results are also provided by recent experimental investigations. For instance, standard rheological measurements were performed on suspensions of small poly(methyl methacrylate) (PMMA) particles sterically stabilized by a coating of poly-12-hydroxystearic acid (14). The suspension was indeed found to follow two separate viscosity curves with distinct critical volume fractions, depending on what shear rate was applied. A similar suspension was investigated under shear reversal (15), during which the viscosity first drops to a low value set by hydrodynamic interactions before increasing to a plateau dominated by contact interactions (16). As expected in such a framework, only the contact contribution to the viscosity increases with increasing shear rate, confirming the key role of contacts in shear-thickening suspensions. Another study reported that in shear-thickening suspensions, the first normal stress difference changes sign at the transition (17). This behavior was interpreted as indicating the formation of frictional contacts between particles, although this point is still a matter of debate (10, 18).

These experimental findings are encouraging; however, they also reflect a major difficulty in testing the frictional transition put forward in the recent theoretical scenario. The standard rheological techniques used, performed under fixed volume fraction, provide information about the suspension shear rate, shear stress, and viscosity. However, they do not give access to the suspension friction coefficient, which is here the key quantity one needs to access. In this article, we propose a different approach inspired by pressure-imposed experiments in granular flows (19), which specifically provides access to the friction coefficient of the

Significance

The sudden and severe increase in the viscosity of certain suspensions above an onset stress is one of the most spectacular phenomena observed in complex fluids. This shear thickening, which has major implications for industry, is a long-standing puzzle in soft-matter physics. Recently, a frictional transition was conjectured to cause this phenomenon. Using experimental concepts from granular physics, we provide direct evidence that such suspensions are frictionless under low confining pressure, which is key to understanding their shear-thickening behavior.

Author contributions: C.C., A.B., B.M., and Y.F. designed research, performed research, analyzed data, and wrote the paper.

The authors declare no conflict of interest.

This article is a PNAS Direct Submission. C.S.O. is a guest editor invited by the Editorial Board.

Freely available online through the PNAS open access option.

Data deposition: Data are now available on the open source database Zenodo at https://doi.org/10.5281/zenodo.556368.

[1]To whom correspondence should be addressed. Email: cecile.clavaud@univ-amu.fr.

suspension. We first compare the quasi-static avalanche angle, compaction, and dilatancy effects, in a standard Newtonian suspension (large glass beads) and a typical shear-thickening suspension (starch particles) flowing under gravity. This comparison reveals that particles in shear-thickening suspensions are frictionless under low confining pressure. Then, to bridge microscopic contact physics to the macroscopic rheology, we use a model suspension (silica beads) where the short-range repulsive force can be tuned. We find that this shear-thickening suspension, which has a frictionless state under low stress, no longer shear thickens when its frictionless state is suppressed.

Results

Steady Avalanches. A simple way to probe the frictional behavior of a suspension is to measure its quasi-static avalanche angle in a rotating drum using nonbuoyant particles (20, 21). For the sake of clarity, we compared the avalanche angle of a standard Newtonian suspension made of large frictional glass beads of diameter $d = 500$ μm (Fig. 1*A*, *Left*), to that of a typical shear-thickening suspension made of potato starch particles ($d = 25$ μm) immersed in water (Fig. 1*A*, *Right*). In both cases, the particle density ρ_p is larger than that of the suspending fluid ρ_f and the fluid viscosity η_f is chosen so that the Stokes number St is low and inertial effects can be neglected ($\mathrm{St} = \sqrt{\rho_p \Delta\rho g d^3}/18\eta_f \sim 10^{-2}$ where $\Delta\rho = \rho_p - \rho_f$ and g stands for gravity) (21). Both suspensions are placed within a rotating drum as shown in the experimental setup illustrated in Fig. 1*B*, *Center*. By imposing a slow and constant rotation speed ω, the nonbuoyant grains at the surface of the pile flow under their own weight, forming a steady avalanche of angle θ on top of a region experiencing a rigid rotation with the drum (20). In such a configuration, the confining pressure acting on the flowing layer of grains is $P = \phi\Delta\rho g h \cos\theta$, where h is the height of the flowing layer and ϕ its volume fraction; the corresponding tangential stress is $\tau = \phi\Delta\rho g h \sin\theta$. In the steady state, the macroscopic friction coefficient of the suspension μ is directly given by the avalanche angle because by definition $\mu = \tau/P = \tan\theta$. The avalanche angle θ thus provides access to the macroscopic friction coefficient of the suspension μ, which itself depends monotonically on the particle friction coefficient μ_p (22). For frictional grains, the macroscopic friction coefficient $\mu \simeq 0.4$ has only a weak dependence on μ_p and yields a typical avalanche angle $\theta \simeq 25^\circ$ (21). However, when the interparticle friction μ_p becomes very small (below 0.1), the macroscopic friction μ sharply drops. However, because of steric constraints, μ remains finite as $\mu_p \to 0$. For frictionless spherical particles ($\mu_p = 0$), discrete simulations predict a quasi-static macroscopic friction $\mu = 0.105$, corresponding to a nonzero avalanche angle $\theta = 5.76^\circ$ (23). Therefore, measuring the pile angle of steady avalanches constitutes a simple, yet decisive way to probe the interparticle friction coefficient in suspensions. Moreover, in this rotating drum configuration, the slope of the avalanche is set by the flowing layer of grains that is located near the free surface of the pile. For the low rotation speeds investigated here, the thickness of the layer h is of the order of a few particle diameters ($h \sim 10\, d$) (24). This means that the measure of the avalanche angle gives access to the frictional state of the grains under very low confining pressure. Typically, for the potato starch particles, the confining pressure within the flowing layer is $P \sim 10\phi\Delta\rho g d \simeq 1$ Pa.

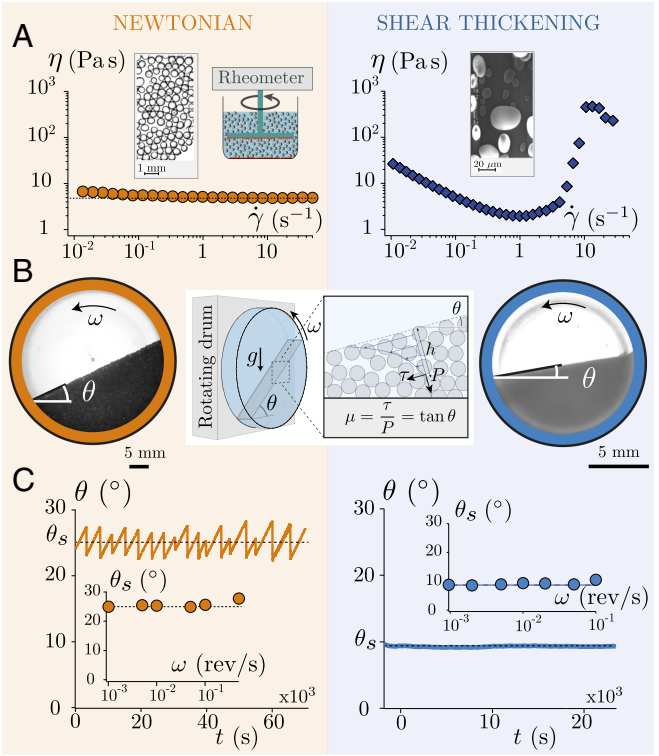

Fig. 1. Steady avalanches in (*Left*) Newtonian and (*Right*) shear thickening suspensions. (*A*) Picture and rheograms (viscosity η vs. shear-rate $\dot{\gamma}$) of (*Left*) a Newtonian suspension of large glass beads ($\phi = 50\%$) and (*Right*) a shear-thickening suspension of potato starch particles ($\phi = 40\%$). Rheograms were obtained in the configuration shown, using density-matched suspensions. (*B*, *Center*) Sketch of the rotating drum. Shown are pictures of a typical steady avalanche for (*B*, *Left*) the glass beads immersed in a mixture of Ucon oil and water and (*B*, *Right*) the potato starch immersed in water. (*C*) Angle of avalanche θ vs. time for (*Left*) the glass beads and (*Right*) the potato starch. (*C*, *Insets*) Steady-state avalanche angle θ_s vs. drum rotation speed ω (see *Materials and Methods* for the detailed description of particles, fluids, and experimental protocol).

Compaction and Dilatancy. Another robust way to probe the frictional behavior of a suspension is to investigate compaction and dilatancy effects (21). The protocol is the following: Particles are first suspended entirely within the drum before being allowed to sediment (Fig. 2*A*). The sediment is then compacted by gently hitting the drum with a rubber-head hammer N_{taps} times. The volume fraction ϕ of the sediment (the ratio of the particle volume to the total volume of the sediment) is measured throughout this compaction process. Finally, the drum is quickly rotated by a fixed angle $\theta_s + 10^\circ$ above the steady-state avalanche angle, to generate a transient avalanche whose angle θ_t is measured vs. time.

For the Newtonian suspension of large glass beads, the avalanche angle θ shows classical hysteretic fluctuations (20) around a time-averaged angle $\theta_s \simeq 25^\circ$ (picture in Fig. 1*B*, *Left* and data in Fig. 1*C*, *Left*). This angle corresponds to a suspension friction coefficient $\mu \simeq 0.47$, which is a usual value for frictional particles. The striking result is that, under the same flowing conditions, the shear-thickening suspension of potato starch particles yields a much lower avalanche angle (picture in Fig. 1*B*, *Right* and data in Fig. 1*C*, *Right*). The suspension can flow steadily with an angle of avalanche as small as $\theta_s \simeq 8.5^\circ$. This angle corresponds to a suspension friction coefficient $\mu \simeq 0.15$, showing that the friction coefficient between particles is nearly vanishing. The suspension friction coefficient ($\mu \simeq 0.15$) here is slightly larger than the expected value for frictionless spheres ($\mu = 0.105$) because potato starch particles are prolate, which geometrically increases the macroscopic friction coefficient (25, 26). Importantly, in the range of drum rotation speeds ω investigated, the avalanche angles reported here do not depend on ω (Fig. 1*C*, *Left* and *Right Insets*). They thus characterize the frictional properties of the suspension in its quasi-static regime, i.e., when the suspension reaches its critical jamming state (9).

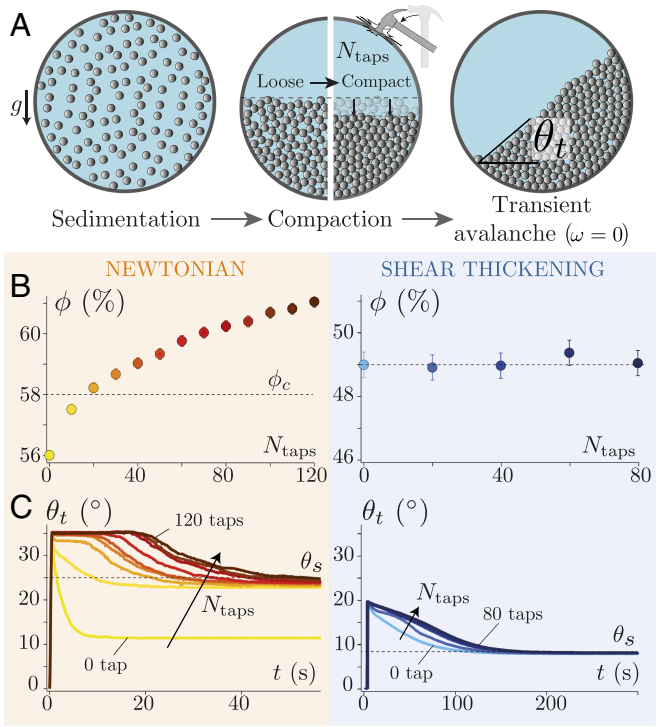

Fig. 2. Compaction and transient avalanches in (*Left*) Newtonian and (*Right*) shear-thickening suspensions. (*A*) Sketch of the experimental protocol to study compaction and dilatancy effects. (*B*) Volume fraction of the sediment ϕ vs. number of taps N_{taps} (*Left*) for the large glass beads and (*Right*) for the potato starch particles. (*C*) Angle of the transient avalanche θ_t vs. time obtained for different initial compactions of the sediment (*Left*) for the large glass beads and (*Right*) for the potato starch particles.

A conspicuous feature of frictional systems, such as a pile of large glass beads, is that it compacts under vibrations. As shown in Fig. 2*B*, *Left*, the packing fraction of the glass beads sediment, which right after sedimentation starts from a loose state ($\phi = 0.56 < \phi_c$), progressively increases with the number of taps to eventually reach a dense state ($\phi = 0.61 > \phi_c$). Remarkably, within this frictional system, very different transient avalanches are observed, depending on the initial preparation of the sediment (Fig. 2*C*, *Left*). For an initial loose packing (0 tap), the avalanche rapidly flows until its angle relaxes to an angle much lower than θ_s (the steady-state avalanche angle measured earlier). Conversely, for an initially compact sediment (120 taps), one observes a long delay during which the avalanche stays still. It then slowly flows, relaxing to θ_s. Such a drastic change in the avalanche dynamics with the packing of the initial sediment relies on a well-known pore pressure feedback mechanism (27–29), which applies only for dilatant (i.e., frictional) systems (23). As first described by Reynolds (30), deformation of a dense granular packing of frictional grains requires its dilation. Thus, as the drum is tilted for the avalanche to flow, the initially compact sediment must dilate. However, dilation in the presence of an incompressible interstitial fluid induces a fluid flow: Some fluid is sucked within the granular network. This fluid flow presses the grains against each other, thereby enhancing friction. As a result, for a compact pile of frictional grains, the avalanche is strongly delayed and then flows slowly, relaxing to θ_s (28, 31). Conversely, a loosely packed granular bed tends to compact when it deforms. This time, the interstitial fluid is expelled from the granular packing, thereby resulting in a fluidization of the grains: The avalanche flows rapidly and relaxes to an angle smaller than θ_s.

The compaction and dilatancy effects observed for the large glass beads are the phenomenological signature of frictional grains. For frictionless particles, the situation is markedly different because there is only one possible state of compaction ($\phi_c = \phi_{rcp}$) and no dilatancy effects are thus expected under shear (23). This is precisely what we observe with the shear-thickening suspension of potato starch particles: Tapping the settled bed of potato starch particles does not modify its packing fraction (Fig. 2*B*, *Right*) and hardly changes the dynamic of the transient avalanches that all relax to θ_s (Fig. 2*C*, *Right*). These experiments again show that, under low confining pressure, potato starch particles behave as if they were frictionless. Note that the maximum packing fraction of the potato starch particles, $\phi = 49\%$, may seem small. However, this low value can be explained by the anisotropic shape of the particles and also their tendency to swell when immersed in water (32).

Tuning Microscopic Friction Using a Model Suspension. We have shown that potato starch particles immersed in water produce a shear-thickening rheology and are frictionless under low confining pressure. These results are consistent with the frictional transition scenario for shear thickening presented in the Introduction (7, 8). They suggest the existence of a short-range repulsion force or a microscopic pressure-dependent friction between the starch particles. However, the origin of this force and more generally the surface physico-chemistry of starch remain unclear (6, 33, 34). To vary the interaction force between particles and investigate the frictional transition within a well-controlled system, we turn to a model suspension composed of silica beads immersed in water (Fig. 3*A*, *Top*). We use non-Brownian silica particles of diameter $d = 24\,\mu m$ comparable in size to the starch particles. When immersed in water, such silica particles spontaneously develop negative surface charges, which generates an electrostatic repulsive force between the grains (35–37). Moreover, this surface charge can easily be screened by dissolving electrolytes (salt) within the solvent. Increasing the salt concentration decreases the range of the repulsive force, i.e., the Debye length λ_D (Fig. 3*A*, *Bottom*), except at very high molarities not considered here (38). This model system is thus particularly appealing to test the recent frictional transition scenario and clarify the link between microscopic interactions between particles, friction, and the suspension macroscopic rheology.

We first use the rotating drum to systematically investigate steady avalanches, compaction, and dilatancy effects on two suspensions of silica beads: one with silica beads immersed in pure water and the second one with the beads immersed in a solution of water and NaCl with a large concentration of salt ($[NaCl] = 0.1$ mol·L^{-1}) to fully screen the Debye layer. Here again inertia is negligible ($St \sim 5 \times 10^{-3}$) and the flowing regime is quasi-static ($\omega \to 0$). As illustrated in Fig. 3 *B–D* (green data), in the presence of a large concentration of salt that screens the repulsive force, the suspension behaves as frictional. The steady-state avalanche angle is large, $\theta_s \simeq 27.5°$; the packing fraction of the sediment evolves from a loose packing right after sedimentation to a dense packing after 60 taps; and the dynamics of the transient avalanche strongly depend on the initial packing, showing features related to the dilatancy effects discussed earlier. [The absolute volume fraction is not reported in Fig. 3 because here it depends on the system size. This size effect can be explained by the large value of the Debye length in pure water ($\lambda_D \simeq 1\,\mu m$), which is not negligible relative to the silica particle diameter (39). Here, particles may be thought of as a hard core of diameter d surrounded by a soft crust of thickness equal to the Debye length. The maximum packing of such a system, when the confining pressure $P \to 0$, is $\phi_{max} \approx \phi_{rcp}(1 - 3\lambda_D/d) \approx 0.48$. However, due to the hydrostatic pressure within the granular bed that depends on the system size, grains deep in the bed must be closer to each other than those at the top. The absolute volume

PHYSICS

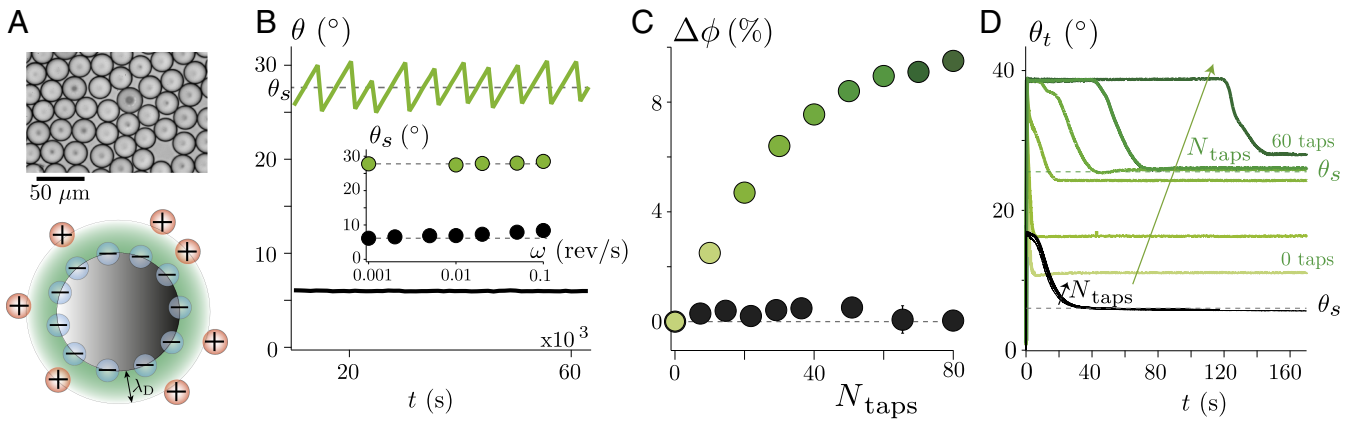

Fig. 3. Steady avalanches, compaction, and dilatancy effects in suspensions of silica beads in (black) pure water or (green) ionic solution. (*A*) Picture of the silica particles and sketch of a silica bead immersed in an ionic solution. Silica particles spontaneously carry negative charges on their surface when immersed in water. The range of the resulting repulsive force, i.e., the Debye length λ_D, can be tuned by changing the ionic concentration of the solvent. (*B–D*) Pile slope avalanche angle θ vs. time (*B*), relative packing fraction of the sediment $\Delta\phi = \phi(N_{taps}) - \phi(N_{taps} = 0)$ vs. number of taps (*C*), and transient avalanche angle θ_t vs. time (*D*) for the silica beads in (green) a sodium chloride solution with [NaCl] $= 0.1$ mol·L^{-1} and in (black) pure water.

fraction may thus lie anywhere between the latter value and 0.64 (random close packing), depending on the system size.] Conversely, the silica beads in pure water behave as frictionless particles (Fig. 3 *B–D*, black data). The steady-state avalanche angle is $\theta_s \simeq 6°$. This value is remarkably close to the quasi-static macroscopic friction angle obtained numerically for ideal frictionless spheres $\theta_s = 5.76° \pm 0.22$ (23). Additionally, no compaction of the granular bed and no discernable effect of the initial packing on the transient avalanches are observed. These results clearly demonstrate that the presence of a short-range repulsive force can lead under low stress to a frictionless behavior of the particles.

To further inquire about the microscopic origin of this frictionless behavior under low stress, we measured the steady avalanche angle θ_s as a function of the salt concentration [NaCl]. Fig. 4*A* shows that the suspension transits progressively from frictionless with $\theta_s \simeq 6°$ in pure water to frictional with $\theta_s \simeq 30°$ when the salt concentration [NaCl] is increased. In addition to this macroscopic measurement, we also characterized the particle roughness with an atomic force microscopy (AFM) and found that the peak roughness of the silica particles is $\ell_r = 3.73 \pm 0.80$ nm. Because the Debye length is entirely set by the salt concentration, $\lambda_D = 0.304/\sqrt{[\mathrm{NaCl}]}$ nm (at $T = 25$ °C) (36), we can plot the steady avalanche angle θ_s as a function of ℓ_r/λ_D (Fig. 4*A*, *Top Inset*). Interestingly, the transition from frictionless to frictional occurs for $\ell_r/\lambda_D \sim 1$. This result strongly supports the idea that the frictionless state arises from the interparticle repulsive force caused by the electrostatic double layer. When its range is smaller than the particle roughness, this force becomes ineffective to prevent the grains from touching and the system is frictional. According to the scenario described in the Introduction (7, 8), the frictional transition should occur when the confining pressure P exerted by the weight of the granular layer equals the critical pressure P_c that the short-range repulsive forces can sustain. Assuming that the repulsive force follows an exponential decay as $F_{\mathrm{rep}}(z) = F_0 \exp(-z/\lambda_D)$ (36), where z is the distance between the particles surfaces, the critical pressure at contact $z = 2\ell_r$ writes $P_c \sim F_{\mathrm{rep}}(2\ell_r)/(\pi d^2/4) \sim (4F_0/\pi d^2)\exp(-2\ell_r/\lambda_D)$. Matching it to the confining pressure $P \sim 10\phi\Delta\rho g d$ predicts a transition when $\ell_r/\lambda_D \sim -(1/2)\log(10\pi\phi\Delta\rho g d^3/4F_0)$. Using $F_0/d \sim 1$ mN/m as reported for silica surfaces in NaCl electrolytes (35) yields $\ell_r/\lambda_D \simeq 1.9$, in fair agreement with the transition observed in Fig. 4*A*.

Finally, we investigate whether for this model suspension, the existence of a frictionless state under low confining pressure leads to a shear-thickening rheology and whether the elimination of this state (by screening repulsive forces) restores a Newtonian behavior. Rheograms of the silica suspensions were obtained using the configuration sketched in Fig. 4*B*, *Inset*. Because silica particles are denser than the aqueous suspending fluid, we used a double helix with tilted blades shearing the entire sample to avoid sedimentation and maintain the homogeneity of the suspension during the measurement. We then define an effective viscosity $\eta_{\mathrm{eff}} = \alpha\Gamma/(2\pi\Omega L^3)$ given by the ratio of the effective stress Γ/L^3, where Γ is the torque and L the helix diameter, to the effective shear rate $2\pi\Omega$ given by the revolution speed Ω of the helix. The constant $\alpha \simeq 0.483$ is set to ensure that the effective viscosity matches the actual viscosity for a Newtonian fluid. We performed rheological measurements on two suspensions of silica particles immersed in water with a salt concentration [NaCl] $= 10^{-4}$mol·L^{-1} and

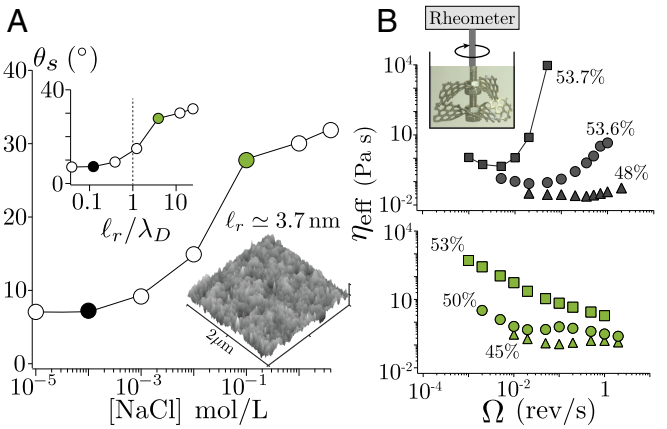

Fig. 4. Frictional transition in silica suspensions when varying the range of the repulsive force and link with macroscopic rheology. (*A*) Steady avalanche angle θ_s vs. salt concentration [NaCl]. (*A*, *Top Inset*) Steady avalanche angle θ_s vs. particle roughness normalized by the Debye length ℓ_r/λ_D. (*A*, *Bottom Inset*) AFM scan of a silica particle surface. The peak roughness is $\ell_r = 3.73 \pm 0.80$ nm. (*B*) Rheograms of silica bead suspensions obtained for different volume fractions in solutions of water and NaCl with salt concentration (*Top*) [NaCl] $= 10^{-4}$ mol·L^{-1} and (*Bottom*) [NaCl] $= 0.1$ mol·L^{-1}. The effective viscosity is $\eta_{\mathrm{eff}} = \alpha\Gamma/(2\pi\Omega L^3)$, where Γ is the torque, Ω is the revolution speed, and $\alpha \simeq 0.483$ is a calibration constant. (*B*, *Inset*) Sketch of the experimental configuration used to obtain the rheograms.

$[\mathrm{NaCl}] = 10^{-1}\mathrm{mol{\cdot}L^{-1}}$, respectively, i.e., just before and after the frictional transition observed in Fig. 4*A*. First, we find that the suspension that has a frictionless state under low confining pressure displays all of the features of a shear-thickening suspension (Fig. 4*B*, *Top*): Continuous shear thickening is observed at moderate volume fractions, whereas larger volume fractions lead to a dramatic increase of its effective viscosity (by about four orders of magnitude). Second, the striking result is that when the repulsive force is screened, so that no frictionless state exists under low confining pressure, the same suspension no longer shear thickens (Fig. 4*B*, *Bottom*). These measurements corroborate previous rheological characterizations using Brownian silica microspheres (17, 40, 41) and confirm the link between the existence of a repulsive force, friction, and shear-thickening rheology.

Discussion

In this article we propose a pressure-imposed approach, inspired from experiments in granular flows, to directly probe the microscopic frictional properties of non-Brownian shear-thickening suspensions. By systematically investigating steady avalanches, compaction, and dilatancy effects in rotating drum experiments, we provide direct proof that shear-thickening suspensions have a frictionless state under low confining pressure. Unlike Newtonian suspensions of frictional particles (9, 20, 28, 29), shear-thickening suspensions under low stress flow with a very small avalanche angle, do not compact, and show no dilatancy effect. This phenomenology clearly indicates the absence of friction between particles (23). Moreover, by using a model suspension of negatively charged silica beads, we find that lowering the range of the repulsive force below that of the particle roughness makes the suspension transit from a frictionless to a frictional state. The elimination of this frictionless state under low confining pressure also suppresses the shear-thickening behavior of the suspension. These experimental results, by linking microscopic contact physics to the suspension macroscopic rheology, provide strong evidence that the frictional transition scenario (7, 8) recently proposed to explain shear thickening applies in real suspensions. For discontinuous shear thickening to occur, the presence of short-range repulsive forces able to prevent interparticle friction at low stress thus seems essential. This picture contrasts with other models of shear thickening in which idealized lubrication hydrodynamics (42), confinement effects (43), particle migration phenomena (44), or inertia (45, 46) were put forward.

The rotating drum configuration used in our study provides a simple, yet robust way to characterize interparticle friction of dense nonbuoyant suspensions. Nevertheless, this configuration also has some limitations. When slowly rotating the drum filled with a nonbuoyant suspension, the thin flowing layer is on top of a pile experiencing solid rotation. Particles thus remain in static contact during long times. For microparticles coated with polymers, which are often involved in shear thickening, these enduring contacts may age and lead to cohesion between grains. In this case, the avalanche angle is no longer constant (47, 48). In our experiments performed with silica particles, small adhesive forces may have affected our results as they could for instance explain the slightly large avalanche angles measured at high salt concentrations (Figs. 3 and 4). However, the transition from low to high avalanche angles must be dominated by frictional effects as (*i*) the steady avalanche angle saturates as the salt concentration is increased, (*ii*) the avalanches have a constant slope from the top to the bottom of the avalanche unlike adhesive powders, and (*iii*) adhesion alone without friction would not lead to the dilatancy effects observed in Fig. 3*D*.

Finally, we emphasize that the rotating drum configuration gives access to the grains' frictional properties in the limit of low confining pressure ($P \to 0$) and in the quasi-static regime, i.e., when the viscous number of the suspension $J = \eta_f \dot{\gamma}/P \to 0$. Interestingly, we were still able to evidence the frictional transition predicted in the recent model by lowering the critical pressure P_c while the confining pressure P remained fixed (Fig. 4*A*). To fully explore the recent models, this transition should also be addressed by varying P while keeping P_c constant and also by varying the viscous number J. Recently, promising devices have been developed, opening the route to pressure-imposed rheometry of dense suspensions, but they are so far limited to the study of macroscopic particles (9). Extending such pressure-imposed approaches to suspensions of shear-thickening and colloidal particles represents a challenging, yet very exciting issue for future studies.

Materials and Methods

Particles. The grains used in Figs. 1 and 2 (*Left*) for the Newtonian suspension are large glass beads of diameter $d = 487 \pm 72$ μm and density $\rho_p = 2{,}500$ kg·m^{-3}. The grains used in Figs. 1 and 2 (*Right*) for the shear-thickening suspension are potato starch particles of major axis $d = 25 \pm 15$ μm and (dry) density $\rho_p = 1{,}500$ kg·m^{-3}. The silica beads used in Figs. 3 and 4 are commercial particles from Microparticles GmbH with diameter 23.46 ± 1.06 μm and density $\rho_p = 1{,}850$ kg·m^{-3}.

Rotating Drum Experiments. The drum used for the large glass beads (Fig. 1*B*, *Left*) has a diameter of 52 mm and a depth of 10 mm with a coarsened side wall. It is filled with a mixture of Ucon oil and pure (microfiltered) water of viscosity $\eta_f = 57$ mPa·s and density $\rho_f = 1{,}005$ kg·m^{-3}. The drum used for potato starch (Fig. 1*B*, *Right*) and silica particles (Figs. 3 and 4) has a diameter of 12 mm and a depth of 3 mm with a coarsened side wall. It is filled with pure water or sodium chloride solutions. Note that to avoid aging of the potato starch, the small drum was surrounded by a thermal bath maintaining its temperature at 7 °C. The drums were mounted on a precision rotating stage (M-061PD from PI piezo-nano positioning). To perform the experiment, the grains were first suspended by rotating the drum at $90° \cdot s^{-1}$. Then, the rotating speed ω was set to the desired value and pictures were taken using a Nikon D300S camera. Compaction experiments in Figs. 2 and 3 consisted of dropping a rubber-head hammer on the drum always from the same height in sequences of 10 taps. Between each sequence, a waiting time was respected to let the system relax. The relative variation of the packing fraction $\Delta\phi$ was inferred by image analysis from the variation of the area of the granular bed.

Rheological Measurements. The rheograms in Fig. 1 were obtained in the configuration sketched in Fig. 1*A*, *Inset*. To perform rheological measurements with a large gap (5 mm) in a plane–plane geometry, the top plate (diameter 50 mm) is fully immersed in the suspension, which itself is contained in a cylindrical vessel (diameter 60 mm). In both cases, the particles were density matched with the suspending fluid to avoid sedimentation. For the large glass beads, the suspending fluid was a mixture of water (30% wt), glycerol (13% wt), and sodium polytungstate (57% wt). For the potato starch, it was a mixture of water (45% wt) and cesium chloride (55% wt). The viscosity is obtained from increasing and decreasing ramps of shear rate after a preshear. No migration effects were noticeable. The rheograms in Fig. 4*B* were obtained in a different configuration because the need to control physico-chemistry (salt concentration) does not allow us to match the suspending fluid density. The configuration, sketched in Fig. 4*B*, *Inset*, uses a double helix with tilted blades of diameter $L = 3$ cm shearing the entire sample to maintain the homogeneity of the suspension during the measurement. The suspension volume fraction is controlled by first letting the particles settle down and adjusting the liquid level at the pile interface, which defined the packing fraction in the loose state, and then adding a given amount of liquid. For each measurement, the suspension is first thoroughly resuspended at a high rotation rate (1 rev/s) while vibrating the container to prevent shear thickening (5). The rotation rate is then set to a given value and the constant torque is measured before the effect of sedimentation is observed. In all cases, torques and rotation rates were measured using an Anton-Paar MCR 501 rheometer.

ACKNOWLEDGMENTS. We are thankful to Sarah Hormozy and Pauline Dame for helping us with preliminary experiments, Alain Rangis from Centre Interdisciplinaire de Nanosciences de Marseille (CINAM) for performing the AFM measurements, and our technical staff at Institut Universitaire des

Systèmes Thermiques et Industriels (IUSTI) for building the experiments. This work was supported by the European Research Council (ERC) under the European Union Horizon 2020 Research and Innovation program (ERC Grant 647384) and by the Labex MEC (ANR-10-LABX-0092) under the A*MIDEX project (ANR-11-IDEX-0001-02) funded by the French government program Investissements d'Avenir.

1. Barnes H (1989) Shear-thickening ("dilatancy") in suspensions of nonaggregating solid particles dispersed in Newtonian liquids. *J Rheol* 33:329–366.
2. Waitukaitis SR, Jaeger HM (2012) Impact-activated solidification of dense suspensions via dynamic jamming fronts. *Nature* 487:205–209.
3. Fernandez N (2014) From tribology to rheology: Impact of interparticle friction in the shear thickening of non-Brownian suspensions. PhD dissertation (ETH–Zürich, Zurich).
4. Wagner NJ, Brady JF (2009) Shear thickening in colloidal dispersions. *Phys Today* 62:27–32.
5. Lin NY, Ness C, Cates ME, Sun J, Cohen I (2016) Tunable shear thickening in suspensions. *Proc Natl Acad Sci USA* 113:10774–10778.
6. Brown E, Jaeger HM (2014) Shear thickening in concentrated suspensions: Phenomenology, mechanisms and relations to jamming. *Rep Prog Phys* 77:046602.
7. Seto R, Mari R, Morris JF, Denn MM (2013) Discontinuous shear thickening of frictional hard-sphere suspensions. *Phys Rev Lett* 111:218301.
8. Wyart M, Cates ME (2014) Discontinuous shear thickening without inertia in dense non-Brownian suspensions. *Phys Rev Lett* 112:098302.
9. Boyer F, Guazzelli É, Pouliquen O (2011) Unifying suspension and granular rheology. *Phys Rev Lett* 107:188301.
10. Mari R, Seto R, Morris JF, Denn MM (2014) Shear thickening, frictionless and frictional rheologies in non-Brownian suspensions. *J Rheol* 58:1693–1724.
11. Lee S, Spencer ND (2008) Sweet, hairy, soft, and slippery. *Science* 319:575–576.
12. Silbert LE (2010) Jamming of frictional spheres and random loose packing. *Soft Matter* 6:2918–2924.
13. Mari R, Seto R, Morris JF, Denn MM (2015) Discontinuous shear thickening in Brownian suspensions by dynamic simulation. *Proc Natl Acad Sci USA* 112:15326–15330.
14. Guy BM, Hermes M, Poon WCK (2015) Towards a unified description of the rheology of hard-particle suspensions. *Phys Rev Lett* 115:088304.
15. Lin NYC, et al. (2015) Hydrodynamic and contact contributions to continuous shear thickening in colloidal suspensions. *Phys Rev Lett* 115:228304.
16. Blanc F, Peters F, Lemaire E (2011) Local transient rheological behavior of concentrated suspensions. *J Rheol* 55:835–854.
17. Royer JR, Blair DL, Hudson SD (2016) Rheological signature of frictional interactions in shear thickening suspensions. *Phys Rev Lett* 116:188301.
18. Cwalina CD, Wagner NJ (2014) Material properties of the shear-thickened state in concentrated near hard-sphere colloidal dispersions. *J Rheol* 58:949–967.
19. Forterre Y, Pouliquen O (2008) Flows of dense granular media. *Annu Rev Fluid Mech* 40:1–24.
20. Courrech du Pont S, Gondret P, Perrin B, Rabaud M (2003) Granular avalanches in fluids. *Phys Rev Lett* 90:044301.
21. Andreotti B, Forterre Y, Pouliquen O (2013) *Granular Media: Between Fluid and Solid* (Cambridge Univ Press, Cambridge, UK).
22. Chialvo S, Sun J, Sundaresan S (2012) Bridging the rheology of granular flows in three regimes. *Phys Rev E* 85:021305.
23. Peyneau PE, Roux JN (2008) Frictionless bead packs have macroscopic friction, but no dilatancy. *Phys Rev E* 78:011307.
24. GDRMiDi (2004) On dense granular flows. *Eur Phys J E Soft Matter* 14:341–365.
25. Azéma E, Radjaï F (2010) Stress-strain behavior and geometrical properties of packings of elongated particles. *Phys Rev E* 81:051304.
26. Guo Y, Wassgren C, Hancock B, Ketterhagen W, Curtis J (2013) Granular shear flows of flat disks and elongated rods without and with friction. *Phys Fluids* 25:063304.
27. Iverson RM (1997) The physics of debris flows. *Rev Geophys* 35:245–296.
28. Pailha M, Nicolas M, Pouliquen O (2008) Initiation of underwater granular avalanches: Influence of the initial volume fraction. *Phys Fluids* 20:111701.
29. Jerome JJS, Vandenberghe N, Forterre Y (2016) Unifying impacts in granular matter from quicksand to cornstarch. *Phys Rev Lett* 117:098003.
30. Reynolds O (1885) LVII. On the dilatancy of media composed of rigid particles in contact. With experimental illustrations. *Philos Mag Ser* 20:469–481.
31. Rondon L, Pouliquen O, Aussillous P (2011) Granular collapse in a fluid: Role of the initial volume fraction. *Phys Fluids* 23:073301.
32. Hellman N, Boesch T, Melvin E (1952) Starch granule swelling in water vapor sorption. *J Am Chem Soc* 74:348–350.
33. Freundlich H, Röder H (1938) Dilatancy and its relation to thixotropy. *Trans Faraday Soc* 34:308–316.
34. Waduge RN, Xu S, Bertoft E, Seetharaman K (2013) Exploring the surface morphology of developing wheat starch granules by using atomic force microscopy. *Starch-Stärke* 65:398–409.
35. Vigil G, Xu Z, Steinberg S, Israelachvili J (1994) Interactions of silica surfaces. *J Colloid Interface Sci* 165:367–385.
36. Israelachvili JN (2011) *Intermolecular and Surface Forces* (Academic, London).
37. Valmacco V, et al. (2016) Dispersion forces acting between silica particles across water: Influence of nanoscale roughness. *Nanoscale Horiz* 1:325–330.
38. Smith AM, Lee AA, Perkin S (2016) The electrostatic screening length in concentrated electrolytes increases with concentration. *J Phys Chem Lett* 7:2157–2163.
39. Watanabe H, et al. (1999) Nonlinear rheology of concentrated spherical silica suspensions: 3. Concentration dependence. *Rheol Acta* 38:2–13.
40. Boersma WH, Laven J, Stein HN (1990) Shear thickening (dilatancy) in concentrated dispersions. *AIChE J* 36:321–332.
41. Lootens D, Van Damme H, Hémar Y, Hébraud P (2005) Dilatant flow of concentrated suspensions of rough particles. *Phys Rev Lett* 95:268302.
42. Phung TN, Brady JF, Bossis G (1996) Stokesian dynamics simulation of Brownian suspensions. *J Fluid Mech* 313:181–207.
43. Brown E, Jaeger HM (2012) The role of dilation and confining stresses in shear thickening of dense suspensions. *J Rheol* 56:875–923.
44. Fall A, et al. (2015) Macroscopic discontinuous shear thickening versus local shear jamming in cornstarch. *Phys Rev Lett* 114:098301.
45. Fall A, Lemaître A, Bertrand F, Bonn D, Ovarlez G (2010) Shear thickening and migration in granular suspensions. *Phys Rev Lett* 105:268303.
46. Fernandez N, et al. (2013) Microscopic mechanism for shear thickening of non-Brownian suspensions. *Phys Rev Lett* 111:108301.
47. Alexander AW, et al. (2006) Avalanching flow of cohesive powders. *Powder Technol* 164:13–21.
48. Liu P, Yang R, Yu A (2011) Dynamics of wet particles in rotating drums: Effect of liquid surface tension. *Phys Fluids* 23:013304.